Received: 1 June 2020 | Revised: 11 September 2020 | Accepted: 2 November 2020

DOI: 10.1002/joc.6925

RESEARCH ARTICLE

International Journal of Climatology RMetS

Multi-year hydroclimatic droughts and pluvials across the conterminous United States

Gregory J. McCabe[1] | **David M. Wolock**[2]

[1]Integrated Modeling and Prediction Division, U.S. Geological Survey, Denver, Colorado

[2]Integrated Modeling and Prediction Division, U.S. Geological Survey, Lawrence, Kansas

Correspondence
Gregory J. McCabe, Integrated Modeling and Prediction Division, U.S. Geological Survey, MS 412 Denver, Colorado 80225.
Email: gmccabe@usgs.gov

Funding information
NOAA Climate Program Office; Office of Biological and Environmental Research (BER); U.S. Department of Energy, Office of Science Innovative and Novel Computational Impact on Theory and Experiment (DOE INCITE); National Oceanic and Atmospheric Administration; U.S. Geological Survey

Abstract

Time series of water-year runoff for 2,109 hydrologic units (HUs) across the conterminous United States (CONUS) for the 1900 through 2014 period were used to identify drought and pluvial (i.e., wet) periods. Characteristics of the drought and pluvial events including frequency, duration, and severity were examined and compared. Additionally, a similar analysis was performed using gridded tree-ring reconstructions of the Palmer Drought Severity Index (PDSI) for the period 1475 through 2005 to place the drought and pluvial characteristics determined using water-year runoff for 1900 through 2014 in the context of multi-century climate variability. The temporal and spatial variability of droughts and pluvials determined using runoff for the 1900 through 2014 period indicated that most drought events in the CONUS occurred before about 1970, whereas most pluvial periods occurred after about 1970. This change in the frequencies of drought and pluvial events around 1970 was largely related to an increase in fall (October through December) precipitation across much of the central United States. Also, the duration and severity of droughts and pluvials identified using runoff for the 1900 through 2014 period generally were not significantly different from the drought and pluvial characteristics identified using the PDSI for the 1475 through 2005 period.

KEYWORDS

climate change, climate variability, multi-year drought, multi-year pluvials, water balance

1 | INTRODUCTION

There is concern that variable precipitation and rising temperature associated with global warming will result in intensified droughts and increases in extreme precipitation events (Rind *et al*., 1990; Hoerling and Eischeid, 2007; Sheffield and Wood, 2008; Dai, 2011a, 2011b, 2013). Higher temperatures also can cause an increase in human water use, particularly because of increases in water demand for agriculture related to increases in evapotranspiration (McDonald and Girvetz, 2013; Blanc *et al*., 2017). For example, groundwater use for irrigation has increased substantially since about 1900 and, in some parts of the conterminous United States (CONUS), has exceeded the natural recharge rates of aquifers (Siebert *et al*., 2010). Also, the rate of groundwater withdrawal for irrigation in the Ogallala (or High Plains) aquifer – the largest aquifer in the CONUS – is almost 10 times the rate of natural recharge, which is causing substantial depletions of this aquifer (Scanlon *et al*., 2010; Scanlon *et al*., 2012; Konikow, 2013; McCabe and Wolock, 2016). In several regions of the United States (U.S.), groundwater depletion increases during droughts, and increases in air temperatures and/or decreases in precipitation likely will

contribute to increased groundwater depletion in the future (Döll, 2009; Russo and Lall, 2017). Additionally, water supplies in some regions of the CONUS, such as the southwestern U.S., are already stressed by increases in consumptive water use, and continued warming likely will add to pressures on water supplies and negatively affect the reliability of water resources (Maupin *et al*., 2014).

One of the first CONUS-wide studies of drought was performed by Karl and Koscielny (1982) who used statewide averages of measured monthly temperature and precipitation to develop time series of monthly Palmer Drought Severity Index (PDSI) values for a grid covering the CONUS; the PDSI is a standardized index of relative wetness and dryness. Using a principal components analysis of the gridded PDSI data, Karl and Koscielny (1982) identified nine regions with similar variability in PDSI. Karl and Koscielny reported that droughts appeared to last longer for the interior portions of the CONUS compared to coastal areas and suggested that this characteristic feature is related to climatic variations across the CONUS. In a subsequent study, Karl (1983) reported that drought lengths for the High Plains and Rocky Mountain states of the CONUS exceed those of areas farther east or west.

Another extensive study of drought in the CONUS was performed by Andreadis *et al*. (2005) who examined the duration, frequency, severity, and extent of both agricultural and hydrologic droughts across the CONUS for the period 1925–2003. In their analyses, Andreadis *et al*. (2005) used model-simulated soil-moisture and runoff to quantify drought and reported that the 1930s, 1950s, and 2000s droughts were the most severe droughts in the CONUS during the 20th century. Andreadis *et al*. (2005) also suggested that severe agricultural droughts are coincident with severe hydrologic droughts.

In contrast to the aforementioned study by Karl and Koscielny (1982), which is based on time series of PDSI, McCabe *et al*. (2016) used a monthly water-balance model to simulate monthly time series of runoff and drought for 2,109 hydrologic units (HUs) in the CONUS for water years 1900 through 2014 (a water year is the period from October 1 of 1 year through September 30 of the following year). Results indicated that (a) the longest mean drought lengths were in parts of the Rocky Mountain region, the northwestern CONUS, and scattered locations across the eastern CONUS; (b) the frequency of drought was highest in the southwestern and central CONUS, and was lowest in the eastern CONUS, the Rocky Mountain region, and the northwestern CONUS; (c) droughts occurred during all months of the year without a seasonal pattern; (d) the variability of precipitation appeared to have been the principal climatic factor determining drought; and (e) for most of the CONUS, drought frequency appeared to have decreased during the 1900 through 2014 period.

In addition to drought studies based on data for the instrumental record (e.g., since about 1900) there have been important drought studies based on paleo-climate reconstructions. For example, Cook *et al*. (1999) developed time series of reconstructions of summer (June through August) PDSI values for a 2° by 3° grid across the CONUS for the period 1700 through 1978. Cook *et al*. (1999) pointed out in their paper that understanding the causes of drought, especially severe multi-year events, is needed to develop reliable forecasting of such events. Additionally, Cook *et al*. (1999) suggested that the use of meteorological measurements to model or forecast U.S. drought is limited temporally and use of paleo-climate reconstructions provides a longer record to analyse. Based on the PDSI reconstructions developed by Cook *et al*. (1999) they concluded that the 1930s "Dust Bowl" drought was the most severe drought in the United States since 1700.

In another paleo-climate analysis of drought, Woodhouse *et al*. (2009) identified two primary drought patterns across the CONUS based on a T-mode principal components analysis (Richman, 1986) of reconstructed PDSI values for the time period 1404 through 2003. One pattern reflected the effects of the El Niño/Southern Oscillation on U.S. hydroclimate and the other indicated an east-to-west dipole.

Although drought events have been the focus of many previous analyses, there have been few analyses that have addressed both dry (i.e., drought) and wet (i.e., pluvial) events. Diaz (1983) used monthly PDSI time series in an analysis of major wet and dry events across the CONUS for 1895 through 1981. Similar to Karl and Koscielny (1982) and Karl (1983), Diaz (1983) reported that the interior and western portions of the CONUS are more prone to drought than are other parts of the CONUS. Diaz (1983) also noted that prolonged wet events tend to occur more frequently in drought-prone areas in the CONUS, resulting in a tendency to be bimodal in moisture conditions (i.e., either too dry or too wet). Kangas and Brown (2007) similarly showed that extreme wet and dry events are more common in the western CONUS than in other U.S. regions.

In an analysis of persistent moisture regimes (wet and dry) across the CONUS using measured (1895 through 1995) and reconstructed (1500 through 1978) PDSI values, Fye *et al*. (2003) compared three notable moisture regimes identified in the measured data (the early 20th century pluvial and the 1930s and 1950s droughts) with moisture regimes identified in the reconstructed PDSI time series. The 20th century pluvial had three analogues in the 16th, 17th, and 19th centuries; however, even though the 16th and 17th century pluvials were of longer duration, the 20th century pluvial was the most extreme

wet episode in the past 500 years. Additionally, the 1930s "Dust Bowl" drought was found to be one of the worst droughts over the western CONUS in the past 500 years, with only the 16th century megadrought being more severe.

Kangas and Brown (2007) also examined droughts and pluvials across the CONUS using PDSI and the Standardized Precipitation Index. Similar to Karl and Koscielny (1982), Diaz (1983) and Kangas and Brown (2007) reported that extreme events (i.e., wet and dry events) are more common in the western CONUS than in other U.S. regions. Kangas and Brown (2007) also reported a decrease in drought area in the CONUS after about 1970.

Few national or regional studies have synthesized instrumental and paleo analyses of both drought and pluvial events. In most previous analyses, these hydrologic events have been examined separately using either the instrumental or paleo record, but not both. In this study, our goal is to examine both drought and pluvial events using the instrumental and paleo record for the CONUS. The broad objectives are to (a) identify areas with similar temporal hydroclimatic variability, (b) identify drought and pluvial events for each region, (c) examine the characteristics of drought and pluvial events (i.e., frequency, duration, severity) for the past century, and (d) place the results for the past century in the context of droughts and pluvial events during the past several centuries using paleo reconstructions of climatic conditions. These results provide an increased understanding of the temporal and spatial variability of both drought and pluvial events across the entire CONUS.

2 | DATA AND METHODS

For this study, droughts and pluvials are identified using water-year runoff. Water-year runoff is computed as total runoff for the 12 months starting on October 1 and ending on September 30 of the following year. Because there are few long-term records of measured runoff across the CONUS, monthly runoff simulated using a monthly water balance model is used in the analyses presented here.

2.1 | The water balance model

Runoff is the climate-driven water supply to an area that is in excess of the evaporative demand (or climatic demand) for water. Simulated runoff from a water balance model is used for this study rather than measured runoff because (a) complete records of measured runoff for the CONUS are limited in both time and space, and (b) the water balance model provides estimates of natural streamflow (or runoff), whereas measured values may be substantially altered by human influences (e.g., dams, diversions, consumptive water use).

Climate inputs to the water balance model are monthly precipitation and temperature. Monthly temperature is used to compute monthly potential evapotranspiration using the Hamon equation (Hamon, 1961). The Hamon potential evapotranspiration equation has been evaluated and compared with a number of other models and is considered a reliable monthly potential evapotranspiration model (Federer *et al*., 1996; Vörösmarty *et al*., 1998; Legates and McCabe, 2005; Lu *et al*., 2005). These previous analyses found that the Hamon model was comparable to more input-detailed models and concluded that the Hamon model produced satisfactory estimates of potential evapotranspiration.

In the water balance model, monthly temperature also is used to determine the proportions of monthly precipitation that are rain and snow. Precipitation that is snow is accumulated in a snow pack.

When rainfall for a month is less than potential evapotranspiration, actual evapotranspiration is equal to the sum of rainfall, snow melt, and the amount of moisture that can be removed from the soil. The fraction of soil-moisture storage that can be removed as actual evapotranspiration decreases with decreasing soil moisture storage; that is, water becomes more difficult to remove from the soil as the soil becomes drier and less moisture is available for actual evapotranspiration. When rainfall (and snow melt) exceeds potential evapotranspiration in a given month, actual evapotranspiration is equal to the potential evapotranspiration; water in excess of potential evapotranspiration replenishes soil-moisture storage. When soil-moisture storage reaches capacity during a given month, the excess water becomes surplus and eventually becomes runoff. Additional details describing the water balance model, its limitations, and goodness-of-fit measures can be found in McCabe and Wolock (2011).

Soil-moisture storage capacity used in the model was computed using the available water-capacity values from the State Soil Geographic Data Base (STATSGO) data set and assuming a 1-m rooting depth. (STATSGO soil data are available at https://www.nrcs.usda.gov/wps/portal/nrcs/site/national/home/.

Monthly temperature and precipitation data were obtained from the Parameter-elevation Regressions on Independent Slopes Model (PRISM) (PRISM Climate Group, Oregon State University, http://www.prism.oregonstate.edu) for the period 1895 through 2014. These data are provided at a 4-km resolution for grid cells across the CONUS and were aggregated to 2,109 U.S.

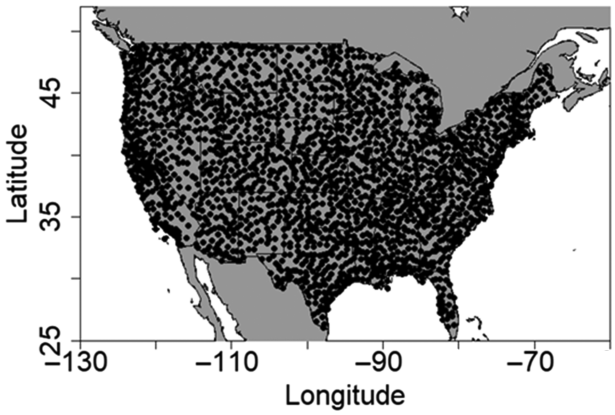

FIGURE 1 Centroids of U.S. Geological Survey 8-digit hydrologic units in the conterminous United States

Geological Survey 8-digit hydrologic units (HUs) (Figure 1). The monthly temperature and precipitation data are used as inputs to the monthly water balance model to estimate time series of monthly runoff.

Because of the sparseness of meteorological data before about 1950, concern has been raised about the use of PRISM monthly temperature and precipitation data for the early part of the 20th century (Gibson et al., 2002; McAfee et al., 2018). However, time series of the monthly PRISM temperature and precipitation data have been used reliably in several previous analyses of runoff for sites across the CONUS (McCabe and Wolock, 2011; Gangopadhyay *et al*., 2015). The use of the monthly PRISM temperature and precipitation data in these previous analyses indicated that the PRISM data are useful for simulating runoff for periods starting as far back as the beginning of the 20th century.

The monthly water balance model was used to simulate time series of monthly runoff for each of the 2,109 HUs for the period 1895 through 2014. Monthly water balance model output for the years 1895 through 1898 were discarded to allow the model time to spin up and to minimize the effects of prescribed initial model conditions; thus, output for 1899 through 2014 was used. The monthly data then were aggregated to compute time series of water-year runoff for each of the HUs.

The water balance model has been evaluated and applied in several previous studies (McCabe and Wolock, 2008; McCabe and Wolock, 2011). These studies include uses of the monthly water balance model for sites across the U.S. and the globe with a range of climatic and physiographic conditions. Monthly water balance estimates of potential evapotranspiration (PET), actual evapotranspiration (AET), and runoff (R) for the PRISM 4-km grid cells for the CONUS are available in a U.S. Geological Survey data release (Wolock and McCabe, 2018).

2.2 | Standardization of runoff time series

The magnitudes of water-year runoff vary substantially across the CONUS. To compare the water-year time series for HUs across the CONUS, the time series of water-year runoff for each HU was standardized by converting the runoff values to percentiles. Converting the time series to percentiles facilitates comparison of the temporal patterns among the 2,109 HUs.

2.3 | Data reduction

The 2,109 time series of water-year runoff percentiles were grouped to examine the temporal variability of water balance components (e.g., precipitation, potential evapotranspiration, actual evapotranspiration, and runoff) more easily. The grouping was achieved using a correlation-based approach to identify sub-regions within the CONUS with similar temporal variability of water-year runoff (McCabe and Wolock, 2016).

The correlation-based clustering process involved the following steps. First, the time series of water-year runoff percentiles for each HU were correlated with time series of water-year runoff percentiles for all other HUs. The HU that was correlated with the most other HUs (at $r \geq 0.5$, $p < .01$) was removed from the original set of HUs along with all the HUs that are correlated with the selected HU above the specified threshold; these HUs compose the first group. A correlation threshold of 0.5 was selected because this threshold has been used in previous analyses and is highly statistically significant given an n value of 2,109. The process is repeated for the remaining HUs to obtain the second and then subsequent groups. The initial classification process resulted in each time series of water-year runoff percentiles for the 2,109 HUs being assigned to one of eight groups. The cutoff at eight groups was selected because continued separation into additional groups resulted in groups that included less than 4% of the 2,109 HUs in any one group.

To ensure that all HUs were assigned to the optimal group, water-year runoff percentiles for each HU in each group were averaged to produce a sub-region average time series of water-year runoff percentiles. Subsequently, the time series of water-year runoff percentiles for each HU then were correlated with each sub-region average series. Each HU was ultimately assigned to the sub-region with which it had the highest correlation. The HUs included in each sub-region are shown in Figure 2. Mean time series of water-year runoff percentiles for each sub-region were computed for subsequent analyses.

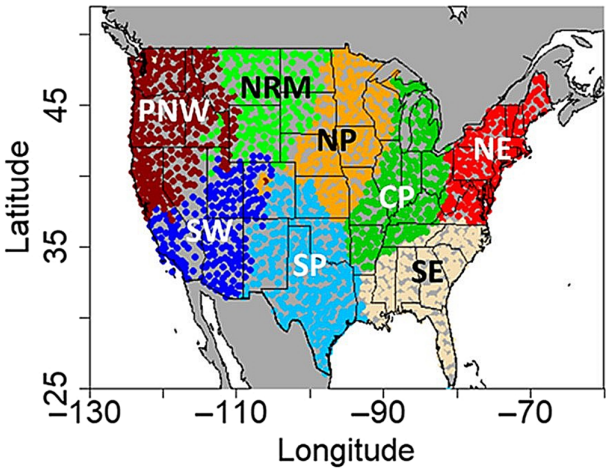

FIGURE 2 Sub-regions of hydrologic units with similar temporal variability in water-year runoff during 1900 through 2014. CP, Central Plains; NE, Northeast; NP, Northern Plains; NRM, North Rocky Mountains; PNW, Pacific Northwest; SE, Southeast; SP, Southern Plains; SW, Southwest

For convenience, the eight sub-regions were named according to geographic regions (Pacific Northwest (PNW), Central Plains (CP), Southeast (SE), Southern Plains (SP), Northeast (NE), Northern Plains (NP), Southwest (SW), and Northern Rocky Mountains (NRM) (Figure 2)). The median correlations between each HU with the respective group average time series ranged from 0.66 ($p < .01$) (NRM sub-region) to 0.71 ($p < .01$) (SE sub-region). The eight sub-regions are similar in size and geographic location as the nine sub-regions identified by Karl and Koscielny (1982). Mean time series of percentiles of water-year runoff for each sub-region were used for subsequent analyses.

The aggregation of runoff data for the sub-regions provides the opportunity to examine drought and pluvial variability for each of the eight sub-regions separately. This is important because causative factors affecting droughts and pluvials can be identified more readily for sub-regions than for a single region as large as the entire CONUS (Namias, 1983).

2.4 | Additional data sets

To identify relations between atmospheric circulation and runoff we used monthly 2° by 2° 700 hPa geopotential height anomalies (in meters [m]) and 700 hPa wind vector anomalies for the region 180° West to 30° West and from 0° to 80° North. The 700 hPa height anomalies were computed using means for the 1900 through 2014 period. Geopotential height data for the 700 hPa level were selected for use in this study because the 700 hPa atmospheric pressure surface provides a useful representation of tropospheric atmospheric circulation that influences seasonal surface weather variations. The monthly 700 hPa data were obtained from the 20th Century Reanalysis Project (Version 3) (Compo *et al.*, 2011).

To place the drought and pluvial events identified for the eight sub-regions during the instrumental period in the context of multi-century climate variability, comparisons were made with drought and pluvial events in previous centuries based on tree-ring reconstructions of summer (June through August) PDSI values in the CONUS (Cook *et al.*, 2010). These reconstructions of the summer PDSI are provided on a 0.5° by 0.5° grid resolution for North America and include 3,237 grid cells located in the CONUS with complete data for the time period 1475 through 2005. The PDSI time series were developed using tree-ring reconstructions up until 1978, after which the PDSI values were computed from instrumental data (Cook *et al.*, 2010). It should be noted that the uncertainty of reconstructed PDSI values increases with the age of the chronology (i.e., the farther back in time), in part, due to fewer tree-ring chronologies on which to base the PDSI estimates.

In keeping with the methodology used to process the runoff data we first converted the time series of PDSI for each of the 3,237 grid cells to percentiles. We subsequently identified the sub-region in which each of the 3,237 PDSI grid cells was located and generated mean time series of PDSI percentiles for each sub-region.

As a verification of the use of PDSI as a proxy for runoff we compared time series of mean percentiles of water-year runoff and PDSI for each sub-region for the years common to both data sets (i.e., 1900 through 2005) (Figure 3). Pearson correlations between the runoff and PDSI time series are statistically significant at $p < .05$ for all sub-regions. The correlation coefficients ranged from 0.59 for the NE sub-region to 0.85 for the SW sub-region, with a median correlation of 0.73 for all sub-regions. These results, and those from previous studies, indicate that PDSI can be used as a proxy to examine inter-annual variability in runoff.

2.5 | Defining drought and pluvial events

Drought and pluvial events were defined using smoothed time series of water-year runoff percentiles for each sub-region. The mean time series of runoff percentiles for each sub-region were smoothed with a 3-year moving average to remove high frequency variability of water-year runoff.

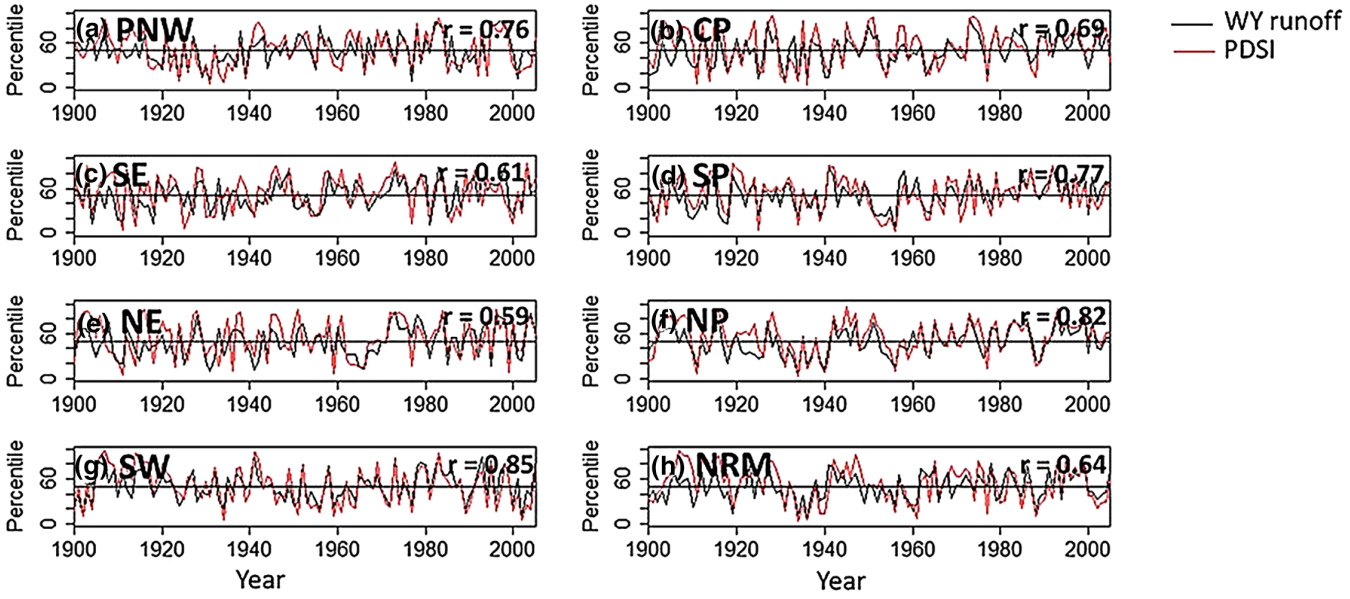

FIGURE 3 Comparison of mean percentiles of water-year (WY) runoff and Palmer Drought Severity Index values for each sub-region (1900–2005). The Pearson correlation (r) between the time series is indicated in bold. CP, Central Plains; NE, Northeast; NP, Northern Plains; NRM, North Rocky Mountains; PNW, Pacific Northwest; SE, Southeast; SP, Southern Plains; SW, Southwest

The "rules" used to determine drought events were as follows:

1. A drought event begins when the smoothed mean sub-regional percentile of water-year runoff is less than the 50th percentile.
2. A drought event ends when the smoothed mean sub-regional percentile of water-year runoff is equal to or greater than the 50th percentile.
3. Only droughts that include three or more consecutive smoothed mean sub-regional percentiles below the 50th percentile were retained for analysis.

Conversely a pluvial event was identified using the rules below:

1. A pluvial event begins when the smoothed mean sub-regional percentile of water-year runoff is equal to or greater than the 50th percentile.
2. A pluvial event ends when the smoothed mean sub-regional percentile of water-year runoff is less than the 50th percentile.
3. Only pluvial events that include three or more consecutive smoothed mean sub-regional percentiles equal to or greater than the 50th percentile were retained for analysis.

For each drought and pluvial event, we computed the length in years (duration) and the mean percentile (severity) during the drought/pluvial event.

Using the "rules" to define droughts and pluvials described above we were able to clearly identify recognizable droughts and pluvials in the instrumental record such as the 1930s and 1950s droughts that affected a large part of the CONUS.

3 | RESULTS AND DISCUSSION

Before quantifying the occurrence and characteristics (e.g., duration and severity) of drought and pluvial events we examined the mean monthly water balances of each sub-region (Figure 4). This involved computing mean monthly values of precipitation, potential evapotranspiration, actual evapotranspiration, and runoff for each of the eight sub-regions. An examination of the mean monthly water balance components for each of the eight sub-regions provides a description of the interaction of mean monthly climatic water supply (i.e., precipitation) with mean monthly climatic demand for water (i.e., potential evapotranspiration) and the resultant partitioning of precipitation into actual evapotranspiration and runoff.

For the PNW sub-region, precipitation is highest from October through April and exceeds potential evapotranspiration during these months (Figure 4a). Additionally, actual evapotranspiration is equal to potential evapotranspiration during these months, whereas actual evapotranspiration is less than potential evapotranspiration from about May through about September. The inter-relations of precipitation and

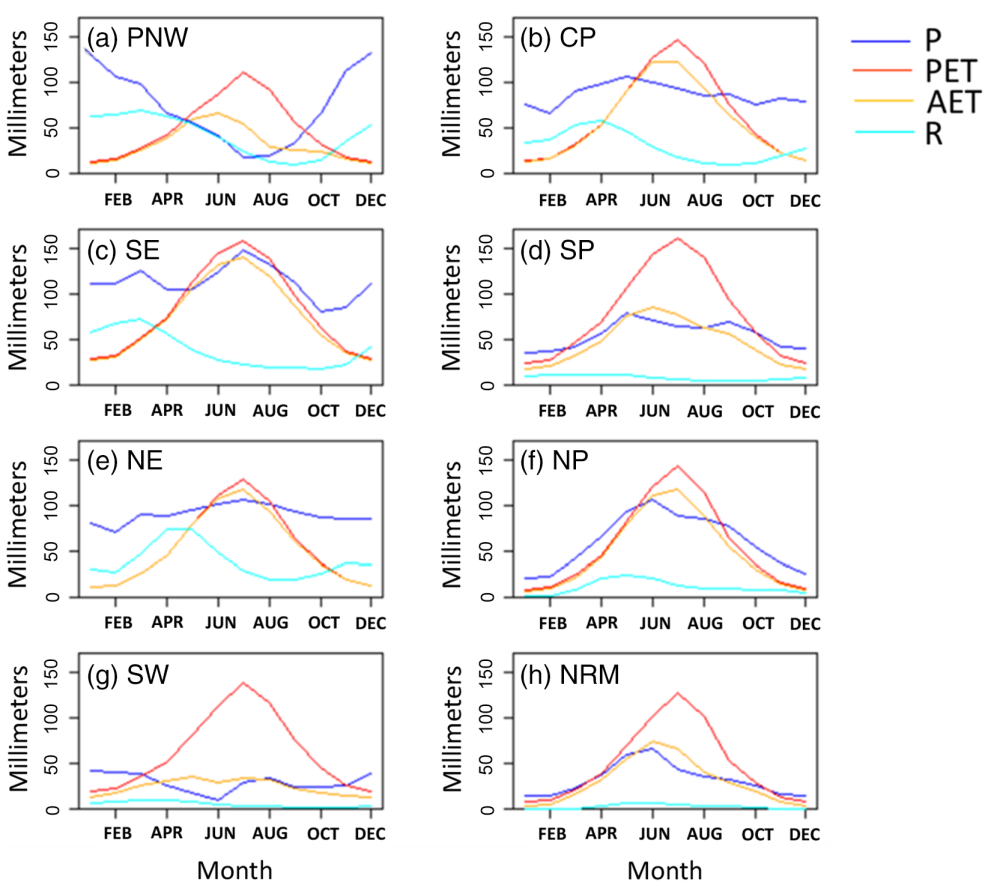

FIGURE 4 Mean monthly water balance components for the 8 sub-regions with similar variability in water year runoff. (P is precipitation, PET is potential evapotranspiration, AET is potential evapotranspiration, actual evapotranspiration, and actual evapotranspiration, R is runoff). CP, Central Plains; NE, Northeast; NP, Northern Plains; NRM, North Rocky Mountains; PNW, Pacific Northwest; SE, Southeast; SP, Southern Plains; SW, Southwest

potential evapotranspiration results in most water-year runoff for sub-region PNW occurring during December through April.

Mean monthly precipitation for the CP sub-region is relatively consistent throughout the year, however, potential evapotranspiration exceeds actual evapotranspiration during the months of June through October (Figure 4b). Most runoff in the CP sub-region is generated during December through June.

Water-year total potential evapotranspiration, precipitation, and actual evapotranspiration for the SE sub-region are the highest values among all eight sub-regions (Figure 4c). Because of the high evaporation rates only about 34% of the water-year precipitation for sub-region SE becomes runoff with over half (~54%) of total water-year runoff for sub-region SE occurring during the months of January through April.

The SP sub-region has one of the lowest water-year runoff values of the eight sub-regions because most of the precipitation becomes actual evapotranspiration (water-year precipitation = 657 mm, and water-year actual evapotranspiration = 556 mm (Table 1)) (Figure 4d). The highest mean monthly runoff for the SP sub-region is only about 12 mm.

Like the CP sub-region (Figure 4b), precipitation for the NE sub-region is consistent throughout the year (Figure 4e). Water-year total actual evapotranspiration for this sub-region is almost equal to water-year total potential evapotranspiration (water-year potential evapotranspiration = 652 mm, water-year actual evapotranspiration = 620 mm [Table 1]). The small difference between water-year potential evapotranspiration and actual evapotranspiration indicates that most of the climatic demand for water for this sub-region is met by precipitation (Figure 4e). Approximately 52% of total water-year runoff occurs during just 4 months (March through June) in the NE sub-region. The highest mean monthly runoff values for the NE sub-region occur during April and May and indicate an effect of snow melt on the timing of monthly runoff (Figure 4e).

The NP sub-region is located in the north-central CONUS (Figure 2) and precipitation is slightly greater than potential evapotranspiration during the cool season months (Figure 4f). Because precipitation and potential evapotranspiration for the NP sub-region are so similar in magnitude throughout the year (water-year precipitation = 719 mm, water-year potential evapotranspiration = 674 mm [Table 1]) only small amounts of runoff are generated in the NP sub-region. Like the NE sub-region (Figure 4e), the peak runoff values for the NP sub-

TABLE 1 Mean water-year precipitation (P), potential evapotranspiration (PET), actual evapotranspiration (AET), runoff (R), and runoff efficiency (RE) for 8 sub-regions in the conterminous United States for 1900 through 2014. Precipitation, potential evapotranspiration, actual evapotranspiration, and runoff are in millimetres, and RE is the ratio of runoff to precipitation. The highest (^{H}) and lowest(^{L}) values for a variable are labelled with superscripts

Sub-region	P	PET	AET	R	RE
PNW	883	572^{L}	380	503^{H}	0.57^{H}
CP	1,038	757	684	353	0.34
SE	1,349^{H}	964^{H}	884^{H}	464	0.34
SP	657	923	556	101	0.15
NE	1,087	652	620	467	0.43
NP	719	674	584	134	0.19
SW	353^{L}	742	289^{L}	64	0.18
NRM	385	580	352	32^{L}	0.08^{L}

Abbreviations: CP, Central Plains; NE, Northeast; NP, Northern Plains; NRM, North Rocky Mountains; PNW, Pacific Northwest; SE, Southeast; SP, Southern Plains; SW, Southwest.

region occur during April through June and indicate the effects of snow melt on runoff timing.

Except for just a few cool season months, potential evapotranspiration exceeds precipitation during most months in the SW sub-region, which results in the generation of small amounts of runoff in the SW sub-region (Figure 4g). Compared with the other sub-regions, the SW sub-region has the second lowest total water-year runoff.

The NRM sub-region has the lowest total water-year runoff of all eight sub-regions (Figure 4h). Almost all of the water-year precipitation becomes water-year actual evapotranspiration (water-year precipitation = 385, water-year actual evapotranspiration = 352 (Table 1)). The largest mean monthly runoff for the NRM sub-region is only about 7 mm and occurs during May and June, which corresponds with the months with the highest values of mean monthly precipitation.

By converting mean monthly runoff for each of the sub-regions into percentiles and then plotting them as Hovmöller diagrams (Hovmöller, 1949) with year on the x-axis and month on the y-axis, wet and dry events become evident (Figure 5). Although some of the drought and pluvial events occurred during specific months or seasons, many of the driest and wettest events occurred during entire years (Figure 5). For example, dry events during the 1920s and the 1940s in the PNW sub-region occurred during all months of the year (Figure 5a). This suggests that defining drought and pluvial events on a water-year time scale is appropriate.

3.1 | Drought and pluvial events

Drought and pluvial events determined for each of the eight sub-regions are illustrated in Figure 6. The number of drought events varied from 6 to 10 for the 8 sub-regions during 1900 through 2014 (Table 2a). The NP sub-region experienced the fewest drought events, whereas the SE, NE, and SW sub-regions suffered the most drought events (Table 2a). The mean length (or duration) of droughts ranged from 5 to 7 years, with the longest single drought event occurring in the SW sub-region (20 years, 1945 through 1964) (Table 2a). Mean drought severity (mean event percentile) among the eight sub-basins ranged from 37 (NP sub-region, the lowest mean percentile) to 42 (PNW sub-region, the least severe mean drought percentile) (Table 2a). The driest single drought event occurred for the SP sub-region (mean percentile of 31) during 1916 through 1918) (Table 2a).

The number of pluvial events among the eight sub-regions ranging from 7 to 10 events (Table 2b). The mean duration of pluvial events ranged from 5 to 8 years, and the maximum pluvial event was 23 years (SP sub-region, 1978–2000). Mean severity ranged from 57 (SP sub-region, least severe mean pluvial) to 61 (CP and SE sub-regions, wettest mean pluvials) (Table 2b). The wettest individual pluvial event (mean percentile of 73) occurred for the PNW sub-region during 1994–1999 (Table 2b).

Most drought events for most of the sub-regions occurred during the decades before the 1970s (Figure 6). In contrast, most of the pluvial events, especially the wettest pluvial events, occurred primarily after about 1970. Time series of counts of the number of sub-regions in a drought or pluvial event illustrated in Figure 7 appear to indicate a decrease in the number of sub-regions in drought, and an increase in the number of sub-regions in a pluvial event after about 1970. Using a Pettit change-point test (Pettit, 1979) with a 95% confidence level we found a change point for the number of drought events at 1966 and a change point for the number of pluvials at 1967. These changes in the occurrence of drought and pluvial events is consistent with a change near 1970 that corresponds with previous studies that have reported an increase in precipitation in the CONUS after about 1970 (Milly and Dunne, 2001; McCabe and Wolock 2002; Seager et al., 2012) and with the results presented by Kangas and Brown (2007), who reported a decrease in drought area in the CONUS after about 1970.

A comparison of the time series of counts of the number of sub-regions in drought or pluvial events (Figure 7) with time series of 3-year moving average U.S. water-year precipitation and temperature indicates that these time series are significantly correlated with the temporal variability of precipitation. The Pearson correlation between

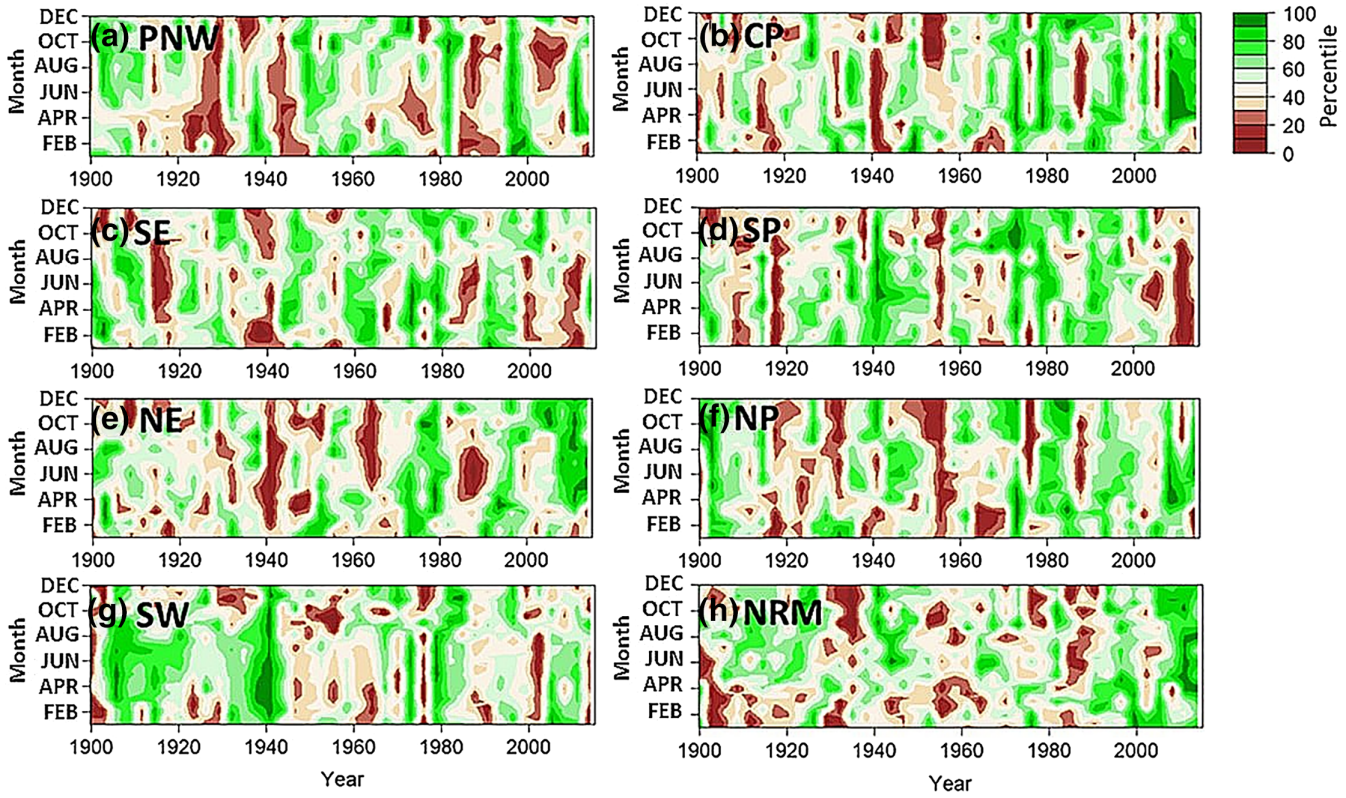

FIGURE 5 Mean percentiles of monthly runoff for each sub-region. CP, Central Plains; NE, Northeast; NP, Northern Plains; NRM, North Rocky Mountains; PNW, Pacific Northwest; SE, Southeast; SP, Southern Plains; SW, Southwest

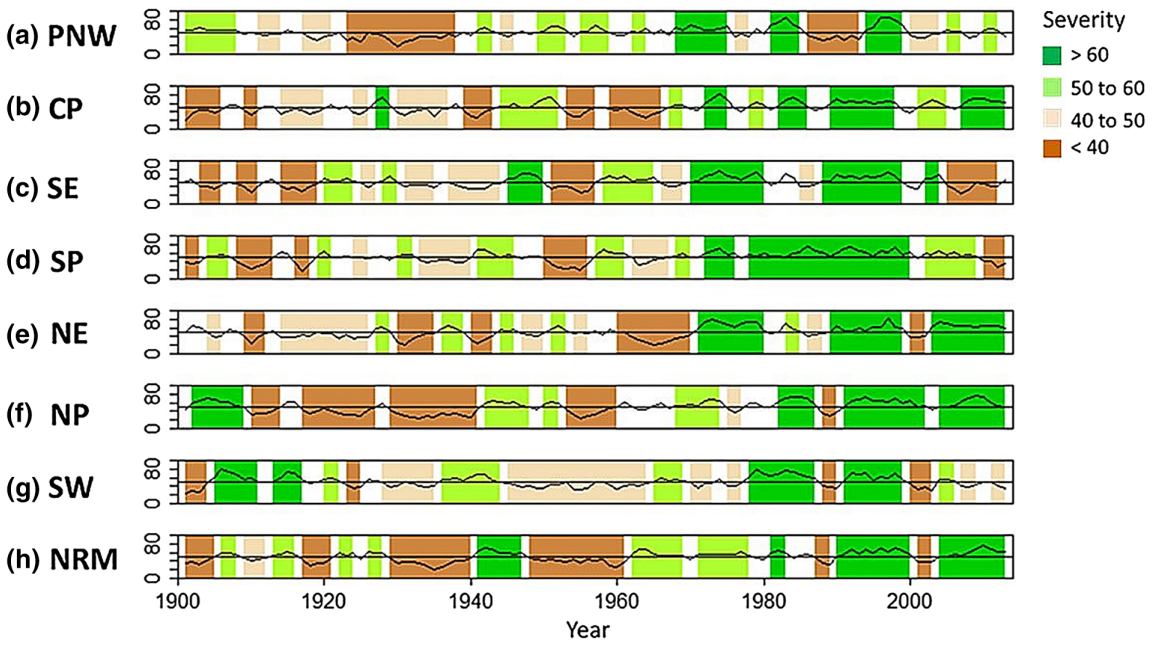

FIGURE 6 Drought (in brown shades) and pluvials (in green shades) for each sub-region computed using percentiles of water-year runoff. CP, Central Plains; NE, Northeast; NP, Northern Plains; NRM, North Rocky Mountains; PNW, Pacific Northwest; SE, Southeast; SP, Southern Plains; SW, Southwest

TABLE 2 Statistics describing characteristics of drought and pluvial events for each sub-region computed using mean sub-region percentiles of water-year runoff for the period 1900 through 2014. The statistics presented are mean duration (in years), mean severity (mean percentile), minimum (min) dur, maximum (max) dur, min sev, max sev, and N (number of drought or pluvial events)

Sub-region	Mean dur	Mean sev	Min dur	Max dur	Min sev	Max sev	*N*
(a) *Drought events*							
PNW	6	42	3	16	37	47	7
CP	6	39	3	8	37	42	8
SE	5	41	3	8	37	46	10
SP	5	38	3	8	31	49	8
NE	5	40	3	13	32	49	10
NP	7	37	3	13	32	42	6
SW	6	40	3	20	32	44	10
NRM	7	39	3	14	36	44	7
(b) *Pluvial events*							
PNW	5	60	3	8	53	73	10
CP	5	61	3	10	54	70	9
SE	7	60	3	12	55	63	7
SP	7	57	3	23	53	62	9
NE	6	60	3	11	55	69	8
NP	8	61	3	12	58	68	7
SW	6	60	3	10	55	68	9
NRM	6	59	3	11	56	62	10

Abbreviations: CP, Central Plains; NE, Northeast; NP, Northern Plains; NRM, North Rocky Mountains; PNW, Pacific Northwest; SE, Southeast; SP, Southern Plains; SW, Southwest.

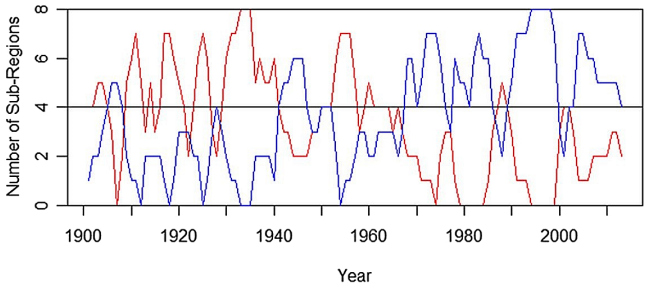

FIGURE 7 The number of sub-regions in a drought event (red line) and in a pluvial event (blue line)

the time series of the counts of the number of sub-regions in a drought event with 3-year moving average CONUS water-year precipitation is −0.87 ($p < .05$), and the Pearson correlation between the time series of the number of sub-regions in a pluvial event with 3-year moving average CONUS water-year precipitation is 0.87 ($p < 0.05$). Pearson correlations of 3-year moving average CONUS water-year temperature with the number of sub-regions in a drought or pluvial event are 0.00 (non-statistically significant) and 0.14 (non-statistically significant), respectively. These results suggest that changes in precipitation around 1970 likely have driven the changes in drought and pluvial conditions around 1970, rather than change in temperature.

To examine precipitation changes across the CONUS around 1970 we performed Student t-tests of seasonal precipitation for the 2,109 HUs. The seasons were defined as follows – fall (October through December [OND]), winter (January through March [JFM]), spring (April through June [AMJ]), and summer (July through September [JAS]). The t-tests identified HUs with statistically significant (at $p < .05$) changes in mean seasonal precipitation for two 20-year periods: water years 1950 through 1969 and water years 1970 through 1989 (Figure 8).

For the fall season, 387 HUs indicate significant increases in precipitation and none of the HUs suggest significant decreases in precipitation (Figure 8a). Most of the HUs that indicate significant increases in fall precipitation are located in an area that extends from the Gulf of Mexico northward to the northern central plains and northern Rocky Mountains.

The number of HUs with significant changes in winter and spring precipitation is smaller than for the fall season and these HUs are widely distributed across the

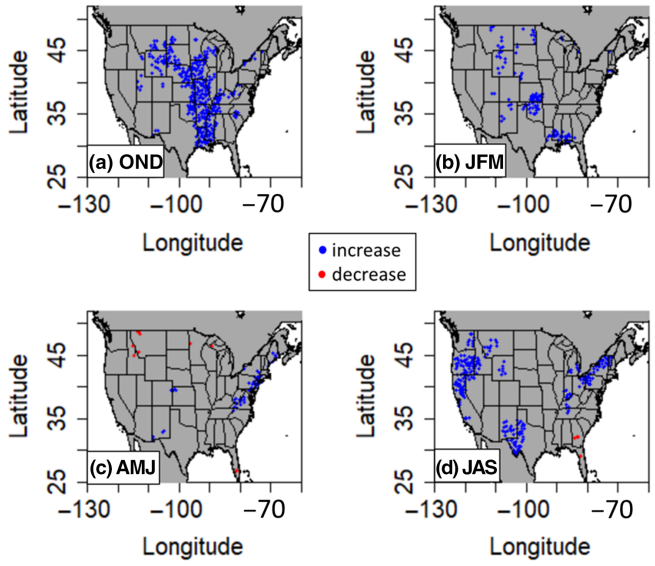

FIGURE 8 Hydrologic units (HUs) with significant changes (at a 95% confidence level) in seasonal precipitation for water years 1971–1990 minus water years 1951–1970. (a) October through December (OND), (b) January through March (JFM), (c) April through June (AMJ), and (d) July through September (JAS). Blue dots indicate HUs with significant increases and red dots indicate HUs with significant decreases

CONUS (Figure 8b,c). For the winter season, 125 HUs indicate significant increases in precipitation and zero HUs suggest significant decreases in precipitation. For the spring season, only 55 HUs indicate significant increases in precipitation and 10 HUs indicate significant decreases in precipitation.

Significant increases in summer precipitation are found for 246 HUs, and significant decreases in summer precipitation are found for only four HUs (Figure 8d). The significant increases in summer precipitation are primarily found for HUs in three regions: (a) the Pacific Northwest, (b) southern New Mexico and western Texas, and (c) part of the northeastern U.S.

These results indicate that there were significant increases in precipitation after about 1970 for many HUs across the CONUS, but only a few HUs experienced significant decreases in seasonal precipitation. Additionally, the fall season had the largest number of HUs with significant increases in precipitation after 1970 and the most geographically coherent pattern of HUs with significant increases in precipitation (Figure 8a). The apparent shift to wetter conditions in the CONUS after 1970 coincides with similar shifts in precipitation and runoff for many locations in the CONUS (McCabe and Wolock, 2002).

Because of the large number of HUs with significant increases in fall precipitation after 1970, we examined changes in fall atmospheric pressures (mean October through December 700 hPa heights) during this period of time to identify possible climatic drivers of these increases in precipitation. The changes in fall 700 hPa heights indicate increases in atmospheric pressures south of Alaska, decreases in atmospheric pressures over the western U.S., and increases in atmospheric pressures over the southeastern U.S. and western North Atlantic Ocean (Figure 9). Also illustrated in Figure 9 are changes in 700 hPa wind vectors and HUs with significant changes in fall precipitation.

The combination of the decreases in fall 700 hPa heights over the western U.S. and the increases in 700 hPa heights over the southeastern U.S. resulted in an enhanced flow of air from the eastern North Pacific Ocean eastward across northern Mexico and then northward from the Gulf of Mexico into the northern central plains (Figure 9). Additionally, the increase in 700 hPa heights over the southeastern U.S. resulted in an enhanced flow of air from the North Atlantic Ocean and Gulf of Mexico into the U.S. (Figure 9). Both of these changes in 700 hPa pressures and associated changes in wind vectors suggest an enhanced flow of moist air into CONUS regions where there are significant increases in fall precipitation. Mo et al. (1997) also reported that this pattern of atmospheric pressure anomalies was associated with wet events in the central U.S. during summer months. Additionally, just east of the negative 700 hPa pressure anomalies over the western U.S. there likely was anomalous positive vorticity advection, which leads to lifting and increased precipitation (Smith *et al.*, 1998). This analysis of changes in 700 hPa pressure heights and wind vectors provides a physical explanation for the increases in fall precipitation.

The apparent shift to wetter conditions in the CONUS after 1970 coincides with similar shifts in precipitation and runoff for many locations in the CONUS (McCabe and Wolock, 2002). The driving factor for the 1970s shift to wetter conditions is not completely clear; however, a recent study by Strong *et al.* (2020) suggests that the increase in precipitation at about 1970 was associated with the development of a pan-Pacific atmospheric wave stemming from deep convection over the warming Indian Ocean. The atmospheric wave moves eastward across the North Pacific Ocean and affects the track and strength of storms over North America.

3.2 | Droughts and pluvials in the context of multi-century climate variability

The drought and pluvial events identified in the instrumental record were placed in a long-term (i.e., multi-century) historical context using tree-ring reconstructions of

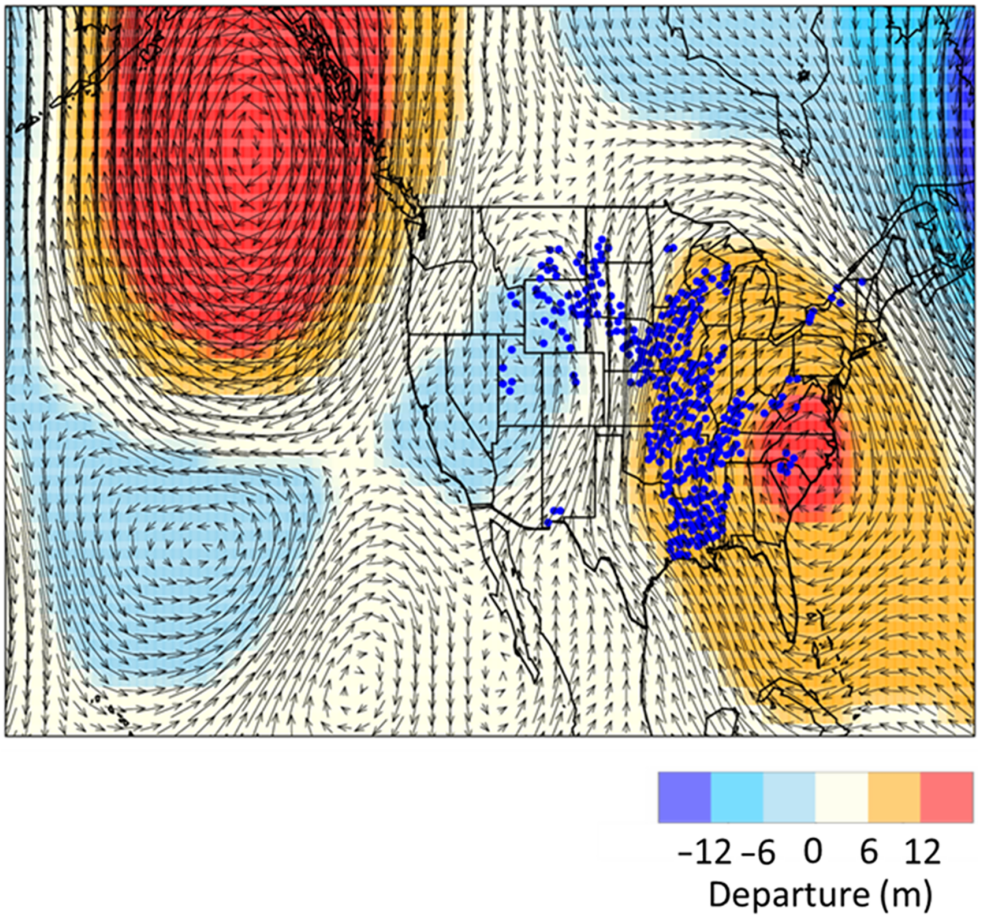

FIGURE 9 Changes (1970–1989 minus 1950–1969) in fall (October through December) 700 hPa heights (in meters [m], shown by colours) and wind vectors (the length of the arrow indicates the magnitude of change in the wind vector), and hydrologic units with significant (at a 95% confidence level) increases in fall precipitation (indicated by blue dots)

PDSI developed by Cook *et al.* (2010). This analysis provided over five centuries of drought and pluvial events for each sub-region (Figure 10). The frequency of drought events for the paleo record ranged from 36 (NRM sub-region) to 52 (SE sub-region) (Table 3). The mean duration of drought events is relatively consistent with a range of 5 years to 7 years (Table 3). The longest droughts for each sub-region ranged from 14 years (PNW sub-region) to 20 years (CP, SP, and SP sub-regions) (Table 3). The driest drought event (with a mean percentile of 24) occurred in the NRM sub-region. Of the 8 sub-regions, the NRM sub-region experienced the largest number of extreme drought statistics: the fewest drought events, longest mean drought duration, driest drought event (Table 3).

The number of pluvial events ranged from 32 (NRM sub-region) to 48 (PNW sub-region) and the mean duration of pluvial events ranged from 5 years (PNW, CP, SP, and NE) to 8 years (NRM sub-region). The longest pluvial event for all sub-regions was 21 years (NRM sub-region) and the most severe pluvial event (highest mean percentile) was 82 for the SW sub-region.

One of the purposes of examining drought and pluvial events for the past several centuries is to put drought during the most recent century in the context of previous centuries. For example, we can address questions such as have drought/pluvial (i.e., duration and severity) characteristics changed through time?

Comparisons of drought duration and severity computed using water-year runoff for 1900 through 2014 and using reconstructed PDSI for 1475–1899 were performed using (a) Student *t*-tests to identify differences in the means of the distribution, and (b) Kolmogorov–Smirnov statistics to examine differences in the distributions of the data. Even though the reconstructed PDSI record extends to 2005, for these comparisons we limited the end point for the PDSI time series to 1899 to avoid overlapping with the time period for the water-year runoff data (i.e., 1900 through 2005).

For drought duration (Figure 11a) there were no statistically significant ($p < .05$) differences in mean drought duration for any of the sub-regions or any statistically significant differences in the distributions of drought duration. These results indicate that drought duration computed for 1900 through 2014 using water-year runoff is similar to drought duration estimated using reconstructed data for 1475 through 1899. For drought severity (mean percentile during a drought

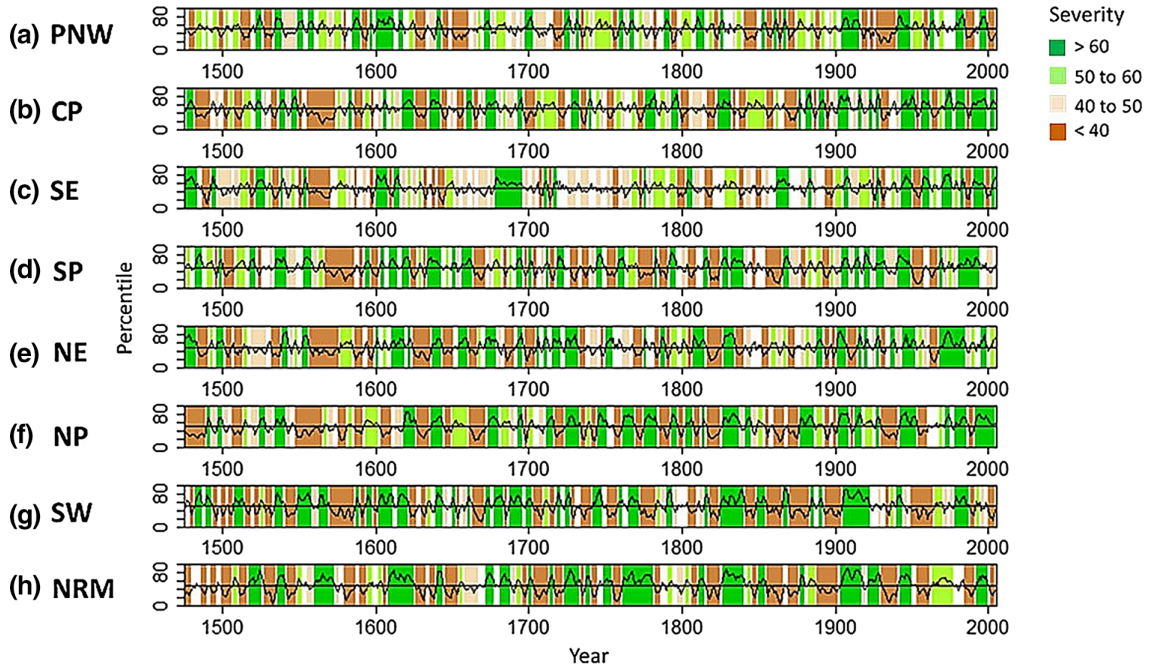

FIGURE 10 Droughts (in brown shades) and pluvials (in green shades) for each sub-region computed using 3-year moving average percentiles of reconstructed PDSI for the period 1475 through 2005. CP, Central Plains; NE, Northeast; NP, Northern Plains; NRM, North Rocky Mountains; PNW, Pacific Northwest; SE, Southeast; SP, Southern Plains; SW, Southwest

TABLE 3 Statistics describing characteristics of drought and pluvial events for each sub-region computed using mean sub-region percentiles of reconstructed Palmer Drought Severity Index values for the period 1475 through 2005. The statistics presented are mean duration (in years), mean severity (mean percentile), minimum (min) dur, maximum (max) dur, min sev, max sev, and N (number of drought or pluvial events)

Sub-region	Mean dur	Mean sev	Min dur	Max dur	Min sev	Max sev	*N*
(a) *Drought events*							
PNW	5	38	3	14	30	47	40
CP	5	39	3	20	29	47	47
SE	5	39	3	16	29	48	52
SP	5	39	3	20	26	46	43
NE	6	38	3	20	27	49	40
NP	6	37	3	19	22	46	39
SW	6	37	3	17	27	46	43
NRM	7	36	3	15	24	46	36
(b) *Pluvial events*							
PNW	5	61	3	13	53	70	48
CP	5	62	3	12	52	74	44
SE	6	61	3	19	53	71	38
SP	5	62	3	15	52	76	44
NE	5	63	3	18	53	77	43
NP	7	63	3	14	54	75	38
SW	6	64	3	19	55	82	39
NRM	8	63	3	21	55	75	32

Abbreviations: CP, Central Plains; NE, Northeast; NP, Northern Plains; NRM, North Rocky Mountains; PNW, Pacific Northwest; SE, Southeast; SP, Southern Plains; SW, Southwest.

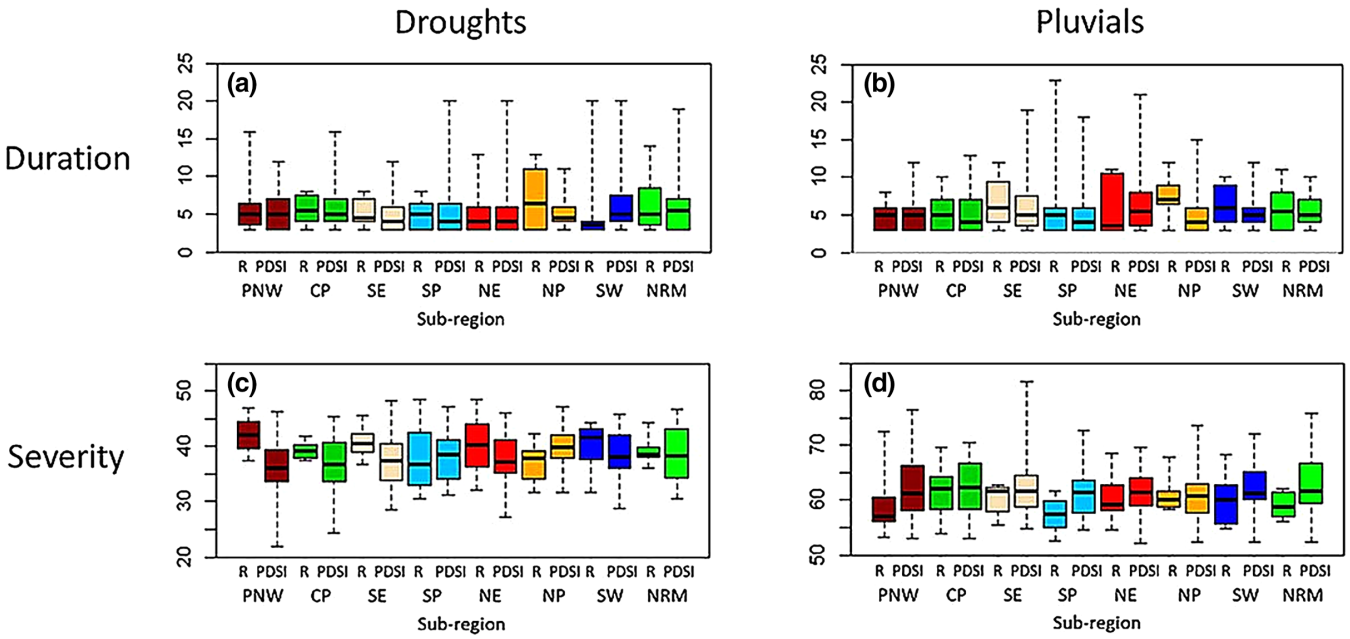

FIGURE 11 Distributions of drought and pluvial duration (in years) and severity (mean percentile) for each sub-region computed using water-year runoff (R) for 1900–2014 and reconstructed Palmer Drought Severity Index (PDSI) for 1475–2005. The distributions are illustrated using box plots, with the heavy black horizontal line indicating the median (i.e., 50th percentile of the distribution), and the top and the bottom of the box indicating the 75th and 25th percentiles respectively. The maximum and minimum percentile values are indicated by the thin lines at the ends of the lines extending upward and downward from the boxes. The colours of the boxes match the colours of the regions in Figure 2. CP, Central Plains; NE, Northeast; NP, Northern Plains; NRM, North Rocky Mountains; PNW, Pacific Northwest; SE, Southeast; SP, Southern plains; SW, Southwest

event) there are statistically significant ($p < .05$) differences in mean drought severity and between the distributions of drought severity for the PNW, CP, and SE sub-regions (Figure 11c). For these three sub-regions, drought events were generally drier (lower mean percentile) for the drought events computed using the reconstructed PDSI data (1475 through 1899) compared to the droughts computed using water-year runoff for 1900 through 2014.

Similar to drought duration, we did not find any statistically significant ($p < .05$) differences in mean pluvial duration, and there was only one sub-region (sub-region NP) with a significant difference in the distributions of pluvial duration between the pluvial events computed using water-year runoff and those computed using reconstructed PDSI (Figure 11b). However, for pluvial severity there are statistically significant ($p < .05$) differences in mean pluvial severity for the SP and NRM sub-regions, and statistically significant differences ($p < .05$) in the distributions of pluvial severity for the PNW sub-region (Figure 11d). This difference is related to the pluvials computed using the reconstructed PDSI for the PNW sub-region being wetter than pluvials computed using water-year runoff for 1900 through 2014.

These results suggest that for most of the CONUS drought/pluvial duration and severity have been relatively constant during the past several centuries.

4 | CONCLUSIONS AND LIMITATIONS

A monthly water balance model was used to simulate time series of water-year runoff for 2,109 U.S. Geological Survey 8-digit hydrologic units (HUs) in the conterminous United States for the period 1900 through 2014. The time series of water-year runoff for the 2,109 HUs were grouped based on similarity in temporal variability in water-year runoff. The clustering process resulted in eight geographically coherent sub-regions of HUs. Mean time series of water-year runoff for these eight sub-regions were used to identify drought and pluvial events for each sub-region and the characteristics (i.e., frequency, duration, severity) of these events were examined and compared. Additionally, a similar analysis was performed for the eight sub-regions using tree-ring reconstructions of the PDSI for the period 1475 through 2005. One of the notable findings from this analysis is that for 1900 through 2014, and across all sub-regions, drought events primarily occurred before about

1970 and pluvial events were most frequent after about 1970. This shift in the frequencies of drought and pluvial events near 1970 was largely related to an increase in fall (October through December) precipitation across much of the central U.S. Also, although there were some droughts and pluvials in the paleo record (i.e., 1475 through 1899) that were longer and more severe than those that were identified using runoff for 1900 through 2014, for the most part the drought and pluvial characteristics (duration and severity) were not significantly different from what occurred during 1900 through 2014.

There is a limitation in our approach concerning one important aspect of drought that we did not address, namely the spatial extent of areas affected by droughts and pluvials. Many notable droughts and pluvials cause great economic harm because of their broad spatial extent. Future analyses will address this important feature of droughts and pluvials.

ACKNOWLEDGEMENTS

The authors thank Ken Eng of the U.S. Geological Survey for helpful comments and suggestions. Atmospheric pressure and wind vector data for the 700 hPa level were obtained from the National Oceanic and Atmospheric Administration (NOAA) Earth System Research Laboratory (https://www.esrl.noaa.gov/psd/data/20thC_Rean/). Support for the Twentieth Century Reanalysis Project data set is provided by the U.S. Department of Energy, Office of Science Innovative and Novel Computational Impact on Theory and Experiment (DOE INCITE) program, and Office of Biological and Environmental Research (BER), and by the NOAA Climate Program Office. The reconstructions of PDSI were obtained from the Living Blended Drought Atlas (LBDA), https://www.ncdc.noaa.gov/paleo-search/study/19119.

ORCID

Gregory J. McCabe https://orcid.org/0000-0002-9258-2997

REFERENCES

Andreadis, K.M., Clark, E.A., Wood, A.W., Hamlet, A.F. and Lettenmaier, D.P. (2005) Twentieth-century drought in the conterminous United States. *Journal of Hydrometeorology*, 6, 985–1001.

Blanc, E., Caron, J., Fant, C. and Monier, E. (2017) Is current irrigation sustainable in the United States? An integrated assessment of climate change impact on water resources and irrigated crop yields. *Earth's Future*, 5, 877–892. https://doi.org/10.1002/2016EF000473.

Compo, G.P., Whitaker, J.S., Sardeshmukh, P.D., Matsui, N., Allan, R.J., Yin, X., Gleason, B.E., Vose, R.S., Rutledge, G., Bessemoulin, P., Brönnimann, S., Brunet, M., Crouthamel, R.I., Grant, A.N., Groisman, P.Y., Jones, P.D., Kruk, M.C., Kruger, A.C., Marshall, G.J., Maugeri, M., Mok, H.Y., Nordli, Ø., Ross, T.F., Trigo, R.M., Wang, X.L., Woodruff, S.D. and Worley, S.J. (2011) The twentieth century reanalysis project. *Quarterly Journal of the Royal Meteorological Society*, 137 (654), 1–28. https://doi.org/10.1002/qj.776.

Cook, E.R., Meko, D.M., Stahle, D.W. and Cleaveland, M.K. (1999) Drought reconstructions for the continental United States. *Journal of Climate*, 12, 1145–1162. https://doi.org/10.1175/1520-0442(1999)012<1145:DRFTCU>2.0.CO;2.

Cook, E.R., Seager, R., Heim, R.R., Vose, R.S., Herweijer, C. and Woodhouse, C. (2010) Megadroughts in North America: placing IPCC projections of hydroclimatic change in a long-term paleoclimate context. *Journal of Quaternary Science*, 25, 48–61. https://doi.org/10.1002/jqs.1303.

Dai, A. (2011a) Drought under global warming: a review. *WIREs Climatic Change*, 2, 45–65.

Dai, A. (2011b) Characteristics and trends in various forms of the palmer drought severity index (PDSI) during 1900–2008. *Journal of Geophysical Research*, 116, D12115.

Dai, A. (2013) Increasing drought under global warming in observations and models. *Nature Climate Change*, 3, 52–58.

Diaz, H.F. (1983) Drought in the United States, some aspects of major dry and wet events in the contiguous United States, 1895-1981. *Journal of Climate and Applied Meteorology*, 22, 3–16.

Döll, P. (2009) Vulnerability to the impact of climate change on renewable groundwater resources: a global-scale assessment. *Environmental Research Letters*, 4, 035006. https://doi.org/10.1088/1748-9326/4/3/035006.

Federer, C.A., Vörösmarty, C. and Fekete, B. (1996) Intercomparison of methods for calculating potential evaporation in regional and global water balance models. *Water Resources Research*, 32, 2315–2321.

Fye, F.K., Stahle, D.W. and Cook, E.R. (2003) Paleoclimatic analogs to twentieth-century moisture regimes across the United States. *Bulletin of the American Meteorological Society*, 84 901–909.

Gangopadhyay, S., McCabe, G.J. and Woodhouse, C.A. (2015) Beyond annual streamflow reconstructions for the Upper Colorado River Basin: A paleo-water-balance approach. *Water Resources Research*, 51, 9763–9774. https://doi.org/10.1002/2015WR017283.

Gibson, W.P., Daly, C., Kittel, T., Nychka, D., Johns, C., Rosenbloom, N., McNab, A. & Taylor, G. (2002) Development of a 103-year high-resolution climate data set for the conterminous United States. *13th Conf. on Applied Climatology, Portland, Oregon, American Meteorological Society*, 181–183.

Hamon, W.R. (1961) Estimating potential evapotranspiration. *Journal of the Hydraulics Division, Proceedings of the American Society of Civil Engineers*, 87, 107–120.

Hoerling, M. and Eischeid, J. (2007) Past peak water in the Southwest. *Southwest Hydrology*, 18-19, 35.

Hovmöller, E. (1949) The trough-and-ridge diagram. *Tellus*, 1, 62–66.

Kangas, R.S. and Brown, T.J. (2007) Characteristics of US drought and pluvials from a high-resolution spatial dataset. *International Journal of Climatology*, 27, 1303–1325. https://doi.org/10.1002/joc.1473.

Karl, T.R. and Koscielny, A.L. (1982) Drought in the United States: 1895-1981. *Journal of Climatology*, 2, 313–329.

Karl, T.R. (1983) Some spatial characteristics of drought duration in the United States. *Journal of Climate and Applied Meteorology*, 22, 1356–1366.

Konikow, L.F. (2013) *Groundwater depletion in the United States (1900–2008). Scientific Investigations Report 2013-5079*. Reston, Virginia: U. S. Geological Survey, p. 63.

Legates, D.R. and McCabe, G.J. (2005) A re-evaluation of the average annual global water balance. *Physical Geography*, 26, 467–479.

Lu, J., Sun, G., McNulty, S.G. and Amataya, D.M. (2005) A comparison of six potential evapotranspiration methods for regional use in the southeastern United States. *Journal of the American Water Resources Association*, 41(3), 621–633.

Maupin, M.A., Kenny, J.F., Hutson, S.S., Lovelace, J.K., Barber, N.L. & Linsey, K.S. (2014) Estimated use of water in the United States in 2010. USGC Circular 1405. Reston, Virginia: U.S. Geological Survey, p. 56. https://doi.org/10.3133/cir1405.

McAfee, S.A., McCabe, G.J., Gray, S.T. & Pederson, G.T. (2018) Changing station coverage impacts temperature trends in the upper Colorado River basin. *International Journal of Climatology*, 39, 1517–1538. https://doi.org/10.1002/JOC.5898.

McCabe, G.J. and Wolock, D.M. (2002) A step increase in streamflow in the conterminous United States. *Geophysical Research Letters*, 29, 2185–38-4. https://doi.org/10.1029/2002GL015999.

McCabe, G.J. and Wolock, D.M. (2008) Joint variability of global runoff and global sea-surface temperatures. *Journal of Hydrometeorology*, 9, 816–824.

McCabe, G.J. and Wolock, D.M. (2011) Independent effects of temperature and precipitation on modeled runoff in the conterminous United States. *Water Resources Research*, 47. https://doi.org/10.1029/2011WR010630.

McCabe, G.J. and Wolock, D.M. (2016) Variability and trends in runoff efficiency in the conterminous United States. *Journal of the American Water Resources Association*, 52, 1046–1055. https://doi.org/10.1111/1752-1688.12431.

McCabe, G.J., Wolock, D.M. and Austin, S.H. (2016) Variability of runoff-based drought conditions in the conterminous United States. *International Journal of Climatology*, 37, 1014–1021. https://doi.org/10.1002/joc.4756.

McDonald, R.I. and Girvetz, E.H. (2013) Two challenges for U.S. irrigation due to climate change: increasing irrigated area in wet states and increasing irrigation rates in dry states. *PLoS One*, 8(6), e65589. https://doi.org/10.1371/journal.pone.0065589.

Mo, K.C., Paegle, J.N. & Higgins, R.W. (1997) Atmospheric processes associated with summer floods and droughts in the central United states. *Journal of Climate*, 10, 3028–3046.

Milly, P.C.D. and Dunne, K.A. (2001) Trends in evaporation and surface cooling in the Mississippi River basin. *Geophysical Research Letters*, 28, 1219–1222.

Namias, J. (1983) Some causes of United States drought. *Journal of Climate and Applied Meteorology*, 22, 30–39.

Pettit, A.N. (1979) A non-parametric approach to the change-point problem. *Applied Statistics*, 28, 126–135.

Richman, M.B. (1986) Rotation of principal components. *International Journal of Climatology*, 6, 293–335.

Rind, D., Goldberg, R., Hansen, J., Rosenzweig, C. and Ruedy, P. (1990) Potential evapotranspiration and the likelihood of future drought. *Journal of Geophysical Research*, 95, 9983–10004.

Russo, T.A. and Lall, U. (2017) Depletion and response of deep groundwater to climate-induced pumping variability. *Nature Geoscience*, 10, 105–108. https://doi.org/10.1038/ngeo2883.

Scanlon, B.R., Reedy, R.C., Gates, J.B. and Gowda, P.H. (2010) Impact of agroecosystems on groundwater resources in the central High Plains, USA. *Agriculture, Ecosystems & Environment*, 139, 700–713. https://doi.org/10.1016/j.agee.2010.10.017.

Scanlon, B.R., Faunt, C.C., Longuevergne, L., Reedy, R.C., Alley, W.M., McGuire, V.L. and McMahon, P.B. (2012) Groundwater depletion and sustainability of irrigation in the US High Plains and Central Valley. *Proceedings of the National Academy of Sciences of the United States of America*, 109, 9320–9325. https://doi.org/10.1073/pnas.1200311109.

Seager, R., Pederson, N., Kushnir, Y., Nakamura, J. and Jurburg, S. (2012) The 1960s drought and the subsequent shift to a wetter climate in the Catskill Mountains region of the New York City watershed. *Journal of Climate*, 25, 6721–6742. https://doi.org/10.1175/JCLI-D-11-00518.1.

Sheffield, J. and Wood, E.F. (2008) Projected changes in drought occurrence under future global warming from multi-model, multi-scenario, IPCC AR4 simulations. *Climate Dynamics*, 31, 79–105. https://doi.org/10.1007/s00382-007-0340-z.

Siebert, S., Burke, J., Faures, J.M., Frenken, K., Hoogeveen, J., Döll, P. and Portmann, F.T. (2010) Groundwater use for irrigation - a global inventory. *Hydrology and Earth System Sciences*, 14, 1863–1880. https://doi.org/10.5194/hess-14-1863-2010.

Smith, S.R., Green, P.M., Leonardi, A.P. and O'brien, J.J. (1998) Role of multiple-level tropospheric circulations in forcing ENSO winter precipitation anomalies. *Monthly Weather Review*, 126, 3102–3116.

Strong, C., McCabe, G. and Weech, A. (2020) Step increase in eastern U.S. precipitation linked to Indian Ocean warming. *Geophysical Research Letters*, 47, e2020GL088911. https://doi.org/10.1029/2020GL088911.

Vörösmarty, C.J., Federer, C.A. and Schloss, A.L. (1998) Potential evaporation functions compared on US watersheds: possible implications for global-scale water balance and terrestrial ecosystem modeling. *Journal of Hydrology*, 207, 147–169.

Wolock D., McCabe GJ (2018) *Water Balance Model Inputs and Outputs for the Conterminous United States, 1900–2015*. U.S. Geological Survey data release. U.S. Geological Survey. https://doi.org/10.5066/F71V5CWN.

Woodhouse, C.A., Russell, J.L. and Cook, E.R. (2009) Two modes of North American drought from instrumental and paleoclimatic data. *Journal of Climate*, 22, 4336–4347. https://doi.org/10.1175/2009JCLI2705.1.

How to cite this article: McCabe GJ, Wolock DM. Multi-year hydroclimatic droughts and pluvials across the conterminous United States. *Int J Climatol*. 2021;41:1731–1746. https://doi.org/10.1002/joc.6925